Xu, W.-L., et al., 2020, Stagnant slab front within the mantle transition zone controls the formation of Cenozoic intracontinental high-Mg andesites in northeast Asia: Geology, v. 48, https://doi.org/10.1130/G47917.1

Stagnant slab front within the mantle transition zone controls the formation of Cenozoic intracontinental high-Mg andesites in NE Asia

Wen-Liang Xu[1*], Jia-Hui Chen[1], Ai-Hua-Weng[2], Jie Tang[1], Feng Wang[1], Chun-Guang Wang[1], Peng Guo[1], Yi-Ni Wang[1], Hao Yang[1], A.A. Sorokin[3]

[1]College of Earth Sciences, Jilin University, Changchun 130061, China

[2] College of Geo-Exploration Science and Technology, Jilin University, Changchun 130061, China

[3]Institute of Geology and Nature Management, Far Eastern Branch of the Russian Academy of Sciences, Blagoveshchensk 675000, Russia

Supplemental Material

Analytical methods, supplementary figures and tables

Analytical methods

1. Mineral electron probe analyses

The mineral phases were performed for major elements on a four-spectrometer Jeol JXA 8100 electron probe microanalyzer in the Key Laboratory of Submarine Geoscience, State Oceanic Administration, using an accelerating potential of 15kV, a beam current of 20nA, a counting time of 20s, and a spot size of 5um. Natural mineral standards and ZAF correction scheme were used for calibration. The analytical results of representative minerals are presented in Table DR1.

2. Whole-rock major and trace element determinations

For geochemical analysis, whole-rock samples were crushed in an agate mill to ~200 mesh. X-ray fluorescence (XRF; Rigaku RIX 2100 spectrometer) using fused glass disks and ICP–MS (Agilent 7500a with a shield torch) were used to measure the major and trace elements compositions, respectively, at the State Key Laboratory of Geological Processes and Mineral Resources, China University of Geosciences, after acid digestion of samples in Teflon bombs. Analytical uncertainties are in the range 1–3%. The analytical results for the BHVO-1 (basalt), BCR-2 (basalt), and AGV-1 (andesite) standards indicate that the analytical precision for major elements is better than 5%, and for trace elements, generally better than 10% (Rudnick et al., 2004). Table DR2 lists the analytical results of major and trace elements for high-Mg andesites in Russian Far East.

3. Sr-Nd-Pb-Hf isotope analyses

Bulk-rock Sr-Nd-Pb-Hf isotope ratios were measured using a Nu Plasma MC-ICP-MS in the Institute of Oceanology, Chinese Academy of Sciences (IOCAS). About 50 mg of rock powder was dissolved with double distilled HNO_3 + HCl + HF in a high-pressure jacket equipped Teflon beaker at 190°C for 15 hours, which was then dried and re-dissolved with 2 ml 3N HNO_3 for 2h. The final sample solution was first loaded onto Sr-spec resin columns to separate Sr and Pb, with the eluted sample solution collected and then loaded onto AG 50W-X8 resin columns to separate REE. The eluted sample solution from AG 50W-X8 resin columns was collected and then loaded onto Ln-spec resin columns to collect Hf. The separated REE solution was dried and re-dissolved with 0.25N HCl before being loaded onto Ln-spec resin columns to collect Nd. The measured $^{87}Sr/^{86}Sr$, $^{143}Nd/^{144}Nd$ and $^{176}Hf/^{177}Hf$ isotope ratios were normalized for instrumental mass fraction using the exponential law to $^{86}Sr/^{88}Sr = 0.1194$, $^{146}Nd/^{144}Nd = 0.7219$ and $^{179}Hf/^{177}Hf = 0.7325$, respectively. International standards of NBS-987, JNdi-1 and Alfa Hf were used as bracketing standards every five samples to monitor the instrument drift during the analysis of Sr, Nd and Hf isotopes, respectively. Repeated analysis for NBS-987 gives the average of $^{87}Sr/^{86}Sr$. Repeated analysis for JNdi-1 gives the average of $^{143}Nd/^{144}Nd$, and repeated analysis for Alfa Hf gives the average of $^{176}Hf/^{177}Hf$. Pb isotope ratios were normalized for instrumental mass fraction relative to NBS/SRM 997 $^{203}Tl/^{205}Tl = 0.41891$. The international

standard NBS-981 was used to monitor the instrument drift during the analysis of Pb isotopes. Repeated analysis of NBS-981 gives the average of $^{206}Pb/^{204}Pb$, $^{207}Pb/^{204}Pb$ and $^{208}Pb/^{204}Pb$. Due to machine damage , the test result of Sr isotope ratio was completed by using TRITON thermoelectric ionization mass spectrometry in Tianjin Geological Survey Center . The main steps of testing Sr sample by TIMS are as follows: take the Nd standard sample of about 100 ng, apply it to the center of Re band after degassing, dry it under the electric current of 0.5A, slowly increase the electric current (about 2.2A) to the Re band in dark red, keep it for 10-20s, then decrease the current and make it cool down. The evaporation band and ionization band are installed on the sample plate and sent to the sample room for testing. During the test, the vacuum of the sample chamber is lower than $9*10^{-8}$ Pa, and the vacuum of the analysis chamber is lower than $9*10^{-9}$ Pa. Generally, the ionization temperature of Sr is about 1250 ~ 1350℃. The ionic flow strength is generally controlled above 5V. The analytical results of Sr-Nd-Pb-Hf isotopes for studied samples are listed in Table DR3.

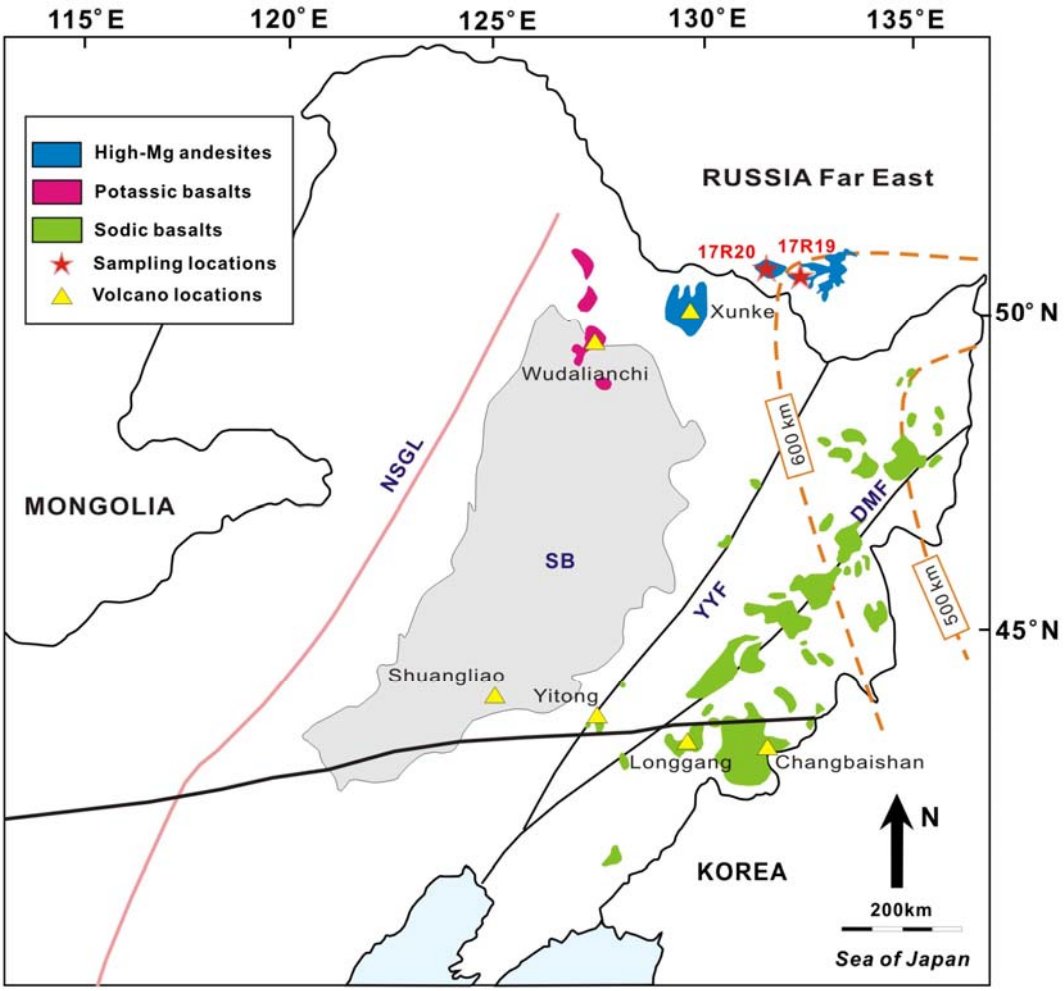

Figure DR1. Distribution map of the Cenozoic volcanic rocks to east of the North-South Gravity Lineament (NSGL). Dashed yellow lines represent the depth of the Wadati–Benioff earthquake zone (Zhao et al., 2009). DMF: Dunhua-Mishan Fault; SB: Songliao Basin; YYF: Yilan-Yitong Fault.

Figure DR2. Representative microphotographs of the Cenozoic intracontinental high-Mg andesites from the Russian Far East. Microphotographs (crossed polarized light) showing the mineral composition, texture and structure of the high-Mg andesites sampled during this study. Abbreviations are as follows: Cpx = clinopyroxene; Ol = olivine; Opx = orthopyroxene; Pl = plagioclase.

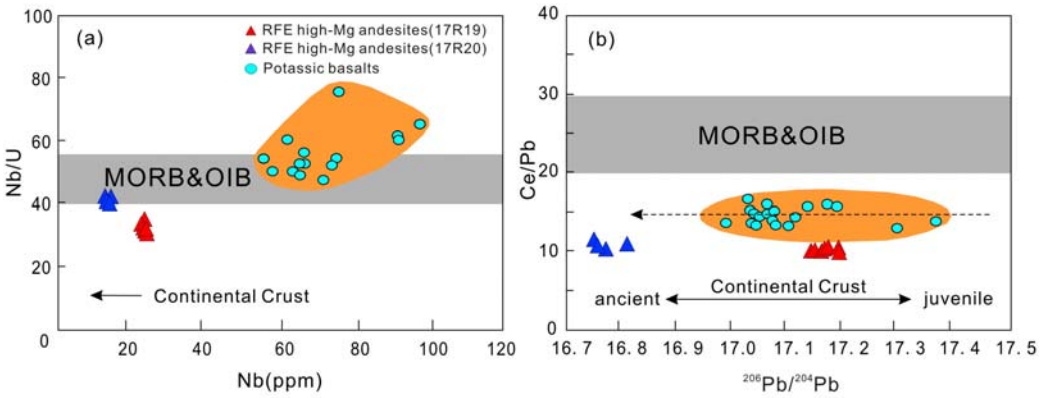

Figure DR3. Plots of Nb/U ratios versus Nb (a) and Ce/Pb ratios versus $^{206}Pb/^{204}Pb$ (b) for the Cenozoic intracontinental high-Mg andesites from the Russian Far East and MORB, OIB, and continental crust (Date from Hofmann et al., 1986). Data of the Cenozoic potassic basalts in NE China from Basu et al. (1991), Zhang et al. (1991, 1995), and Zou et al. (2003).

Text S1

Text S1 Petro-physical constraints of the anomalies beneath NE China

To estimate water content and its possible derived partial melting in the asthenosphere, we can follow steps bellow:

1. Water content and its uncertainty are estimated for the resistivity and temperature at a certain depth according to (Gardés et al., 2014) (**Fig DR4**);

2. Constructing local geotherm from Ichiki et al. (2006) (**Fig DR5**);

3. Water storage capacity at the same depth is estimated according to (Hirschmann et al., 2009) after **Fig DR5**;

4. If estimated water content is less than the corresponding storage capacity, partial melting cannot be triggered, we will use water to interpret low resistivity anomaly. Otherwise, partial melting can occur and we go to next step;

5. Using the water storage capacity and the partition coefficient in (Dmantle/melt=0.006) (Hirschmann et al., 2009) to estimate water content in molten phase, from which and considering local geothermal temperature, we estimate melt conductivity by (Ni et al., 2011);

6. Using dual-phase mixed formula from (Dulien, 1979) with 0.01 S/m as matrix conductivity, the melting fraction could be evaluated.

Thea above steps could be applied to interpret the resistivity of anomalies A, B and C at depth about 325 km. The water content and possible melting fractions are estimated and listed in the **Table DR7**.

Table DR7 Summary of the rock-physics parameters of the detected anomalies.

Anomaly	Type	Pressure and Temperature				Observed Resistivity			H_2O in Peridotite (ppm)	σ_{melt} (S/m)	σ_{host} (S/m)	Archies's Law		Melting Fractions Φ(vol%)
		Depth/GPa	Temp/°C	Water storage capacity (ppm)	Water in melt(wt%.)	ρ_{min} (Ωm)	ρ_{max} (Ωm)	ρ_{avg} (Ωm)				A	n	
A	Basaltic melt	300-350/ ~12	1350[3]	~800[2]	13.3[2]	<3	-	-	~2000[1]	80[4]	0.01	-	-	~1.2[5]
B	Basaltic melt	300-350/ ~12	1350[3]	~800[2]	13.3[2]	<5	-	-	~1200[1]	80[4]	0.01	-	-	~0.7[5]
C	Water plume	300-350/ ~12	1350[3]	800[2]	13.3[2]	<10	-	-	~700[1]	80[4]	0.01	-	-	-

[1] General formula for peridotite conductivity from Ref. (Gardés et al.,2014).

[2] Water content in melt using partition coefficients $D^{mantle/melt}$ = 0.006 from Ref. (Hirschmann et al., 2009).

[3] Geothermal temperature from Ref. (Ichiki et al., 2006).

[4] Basaltic melt conductivity from Ref. (Ni et al., 2011).

[5] Lower crust and mantle: dual-phase mixed formula from Ref. (Dulien, 1979).

Fig.DR4

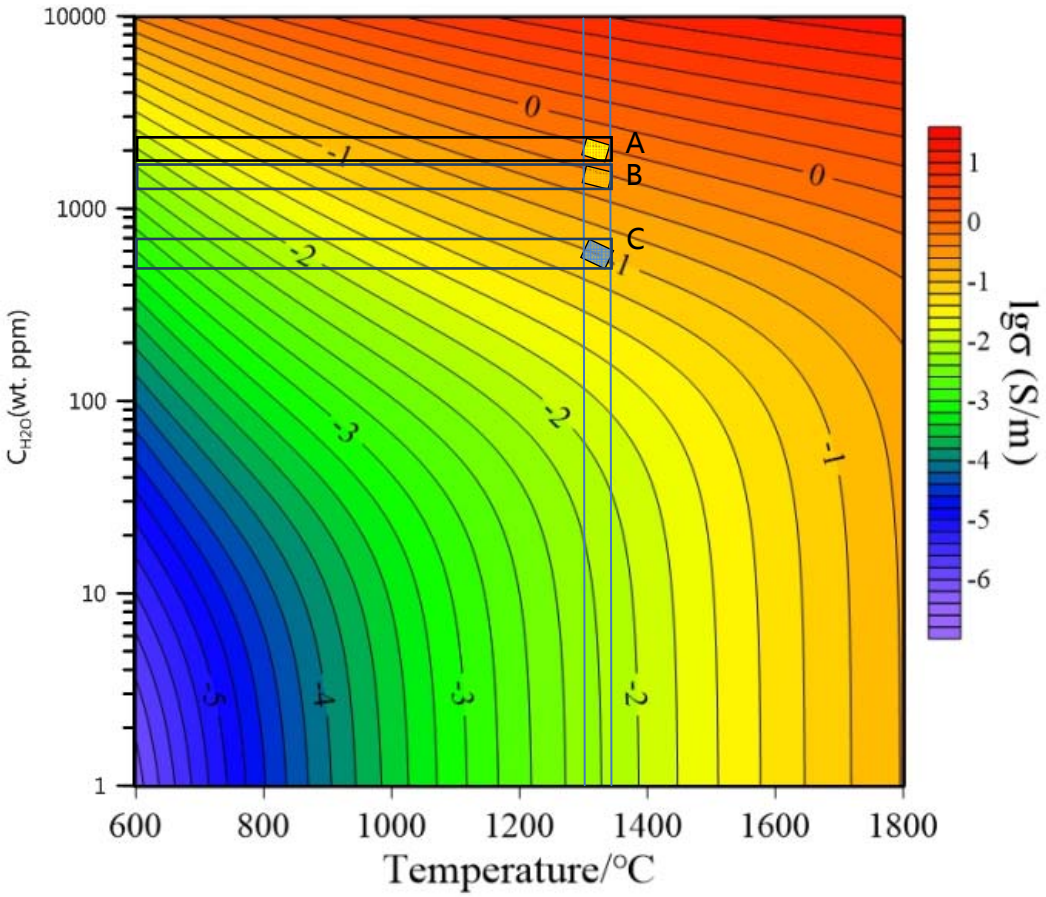

Fig.DR4. Bulk resistivity (in log units) of olivine as a function of temperature and water content (Gardés et al.,2014). Resistivities at the center of anomalies A, B and C are as low as 3, 5, and 10 Ω·m at 350 km depth where the geotherm temperature is estimated to be about 1350 °C (Ichiki et al., 2006**)**.

Fig.DR5

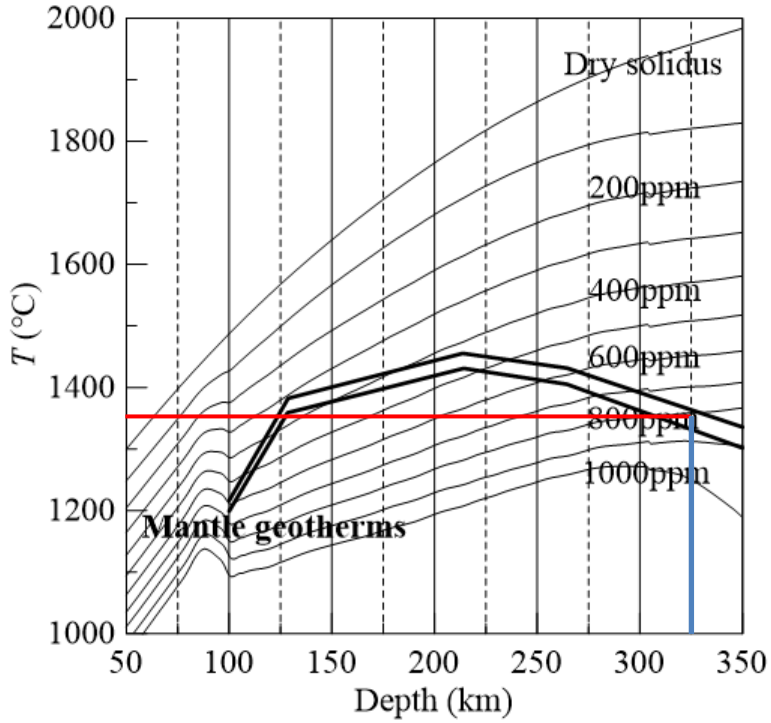

Fig.DR5. Peridotite water storage capacity beneath NE China. Peridotite solidus (thin lines) at different water content (Hirschmann et al,2009). Thick solid lines are the upper and lower bounds of the wave velocity derived geotherm beneath NE China (Ichiki et al., 2006). Water storage capacity in asthenosphere beneath NE China could be read from the cross-points of the geothermal curves with solidus lines at different water content. Water storage capacity is a water content when exceeding this content partial melting will occur, and once partial melting onset, most water in mantle rock will partition into melt, leaving a dry matrix. Water storage capacity increase with pressure, but is also affected by temperature. For example, at the base of asthenosphere where temperature is 1350 °C, the water storage capacity rises to ~800ppm. However, if using normal geothermal, about 1400 °C, it will drop to ~500ppm.

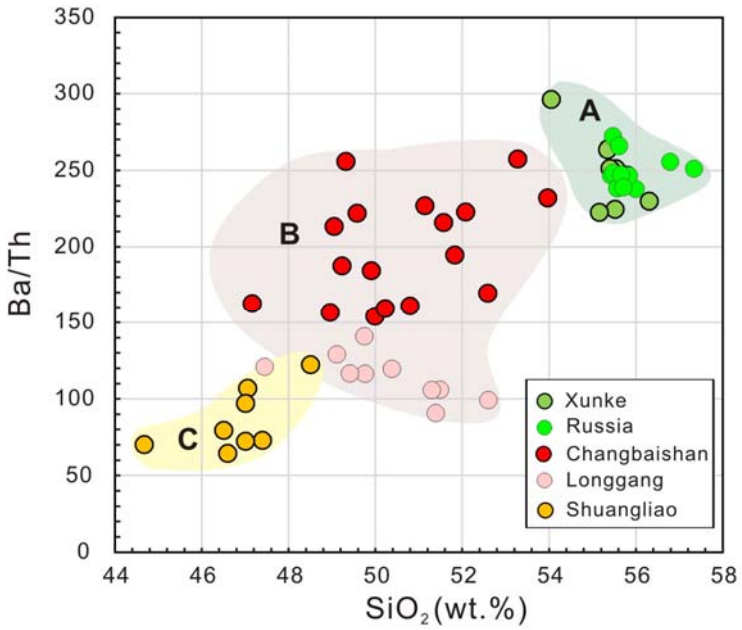

Fig.DR6. Plot of Ba/Th versus SiO_2 for the Cenozoic volcanic rocks corresponding for three low-resistivity anomalies A, B, C in NE Asia. Generally, Ba/Th ratios of volcanic rocks in arcs have positive correlation with water content in magma sources (Chen et al., 2017). The Cenozoic intracontinental HMAs in NE Asia related to anomaly A have the largest Ba/Th ratios (238-273) and the highest SiO_2 contents (55.4%–57.3%), implying their highest water content; the Changbaishan and Longgang sodic basalts related to anomaly B have moderate Ba/Th ratios (90-266) and SiO_2 contents (46.2%–53.9%), i.e., moderate water content; whereas the Shuangliao sodic basalts related to anomaly C exhibit the lowest Ba/Th ratios (64-122) and SiO_2 contents (42.8%–48.5%), i.e., the lowest water content.

SUPPLEMENTARY REFERENCES

Basu, A.R., Wang, J.W., Huang, W.K., Xie, G.H., Tatsumoto, M., 1991, Major element, REE, and Pb, Nd and Sr isotopic geochemistry of Cenozoic volcanic rocks of eastern China: implications for their origin from suboceanic-type mantle reservoirs: Earth and Planetary Science Letters, v. 105, p.149-169, https://doi: 10.1016/0012-821X(91)90127-4.

Chen, H., Xia, Q.K., Ingrin, J., Deloule, E., Bi, Y., 2017, Heterogeneous source components of intraplate basalts from NE China induced by the ongoing Pacific slab subduction: Earth and Planetary Science Letters, v.459, p. 208-220, http://dx.doi.org/10.1016/j.epsl.2016.11.030

Dulien, F.A.L., 1979, Porous Media: Fluid transport and pore structure. Academic Press, New York, pp. 396.

Hirschmann, M.M., Tenner, T., Aubaud, C., Withers, A.C., Pepi, P., 2009, Dehydration melting of nominally anhydrous mantle: The primacy of partitioning. Physics of the Earth and Planetary Interiors, v. 176, p. 54–68, https://doi:10.1016/j.pepi.2009.04.001.

Hofmann, A.-W., Jochum, K.-P., Seufert, M., White, W.-M., 1986, Nb and Pb in oceanic basalts: new constraints on mantle evolution: Earth and Planetary Science Letters, v. 79: p. 33-45, https://doi.10.1016/0012- 821x(86)90038 -5.

Ma, Q., Xu, Y. G., Zheng, J. P., Griffin, W. L., Hong, L. B., & Ma, L., 2016, Coexisting Early Cretaceous high‐Mg andesites and adakitic rocks in the North China Craton: The role of water in intraplate magmatism and cratonic destruction: Journal of Petrology, v. 57(7), p. 1279–1308, https://doi.org/10.1093/petrology/ egw040.

Ni, H. W., Keppler, H. & Behrens, H., 2011, Electrical conductivity of hydrous basaltic melts: implications for partial melting in the upper mantle: Contributions to Mineralogy and Petrology, v.162, p. 637-650,

https://doi:10.1007/s00410-011- 0617-4.

Rudnick, R. L., Gao, S., Ling, W. L., Liu, Y. S., McDonough, W. F., 2004, Petrology and geochemistry of spinel peridotite xenoliths from Hannuoba and Qixia, North China Craton: Lithos, v. 77, p. 609-637, https://doi: 10.1016/j.lithos.2004.03.033.

Zhang, M., Menzies, M.A., Suddaby, P., Thirlwall, M.F., 1991, EM1 signature from within the post-Archaean subcontinental lithospheric mantle: isotopic evidence from the potassic volcanic rocks in NE China: Geochemical Journal, v. 25, p. 387–398, https://doi:10.2343/geochemj.25.387.

Zhang, M., Suddaby, P., Thompson, R.N., Thirlwall, M.F.,Menzies,M.A., 1995, Potassic volcanic rocks in NE China: geochemical constraints onmantle source and magma genesis: Journal of Petrology, v. 36, p.1275–1303, https://doi.org/ 10.1093/petrology/36.5.1275.

Zou, H., Fan, Q. & Yao, Y., 2008, U–Th systematic of dispersed young volcanoes in NE China: asthenosphere upwelling caused by pilling up and upward thickening of stagnant Pacific slab: Chemical Geology, v. 255, p.134–142, https://doi:10.1016/j.chemgeo.2008.06.022.

Zou, H., Reid, M.R., Liu, Y., Yao, Y., Xu, X., Fan, Q., 2003, Constraints on the origin of historic potassic basalts fromnortheast China by U\Th disequilibrium data: Chemical Geology, v. 200, p.189–201, https://doi. 10.1016/S0009-2541(03) 00188-8.

Table DR1 Mineral chemical data (wt.%) for the Cenozoic intracontinental high-Mg andesites from the Russian Far East

Table DR2 Major (wt%) and trace elements (ppm) data for the Cenozoic intracontinental high-Mg andesites from the Russian Far East

Table DR3 Sr-Nd-Hf-Pb isotopic data of the Cenozoic intracontinental high-Mg andesites from the Russian Far East

Table DR4 Geochemical characteristics of some high-Mg andesites (wt.%) from subduction zones

Table DR5 Compared Sr-Nd-Pb isotopic data from intraplate basalts in NE China and andesites in arcs

Table DR6 Present-day compositions of the end-member components

Table DR1 Mineral chemical data (wt.%) for the Cenozoic intracontinental high-Mg andesites from Russian Far East

Sample	17R19-2					17R19-5				17R20-2						17R20-3			
	19-2-1	19-2-2	19-2-3	19-2-4	19-2-5	19-5-1	19-5-2	19-5-3	19-5-4	20-2-1	20-2-2	20-2-4	20-2-5	20-2-6	20-2-7	20-3-1	20-3-2	20-3-3	20-3-4
Mineral	Ol	Ol	Ol	Pl	Ol	Ol	Ol	Pl	Ol	Ol	Ol	Pl (r)	Pl (c)	Cpx (c)	Cpx(C)	Opx (C)	Pl (C)	Pl (r)	Opx (r)
SiO_2	39.50	38.89	39.02	55.91	38.95	39.16	39.41	56.91	39.01	40.03	38.63	56.32	55.68	52.25	52.14	54.32	54.66	57.09	54.33
TiO_2	0.03	-	-	0.09	-	0.02	-	0.11	-	-	-	0.06	0.03	0.82	0.82	0.28	0.06	0.04	0.33
Al_2O_3	0.08	0.04	0.02	26.65	0.03	0.06	0.03	26.01	-	0.04	0.02	26.84	26.96	1.75	2.09	2.40	27.48	26.14	1.32
Cr_2O_3	0.03	0.02	0.05	0.02	0.04	0.06	0.02	-	0.01	0.01	0.02	0.01	0.04	0.11	0.29	0.35	-	0.02	0.45
FeO	17.87	20.34	16.65	0.75	19.91	17.30	17.99	0.57	19.87	14.94	23.20	0.33	0.53	12.26	10.14	12.54	0.72	0.40	14.40
MnO	0.27	0.28	0.22	0.03	0.27	0.23	0.28	-	0.24	0.15	0.31	-	0.01	0.32	0.27	0.26	-	0.01	0.28
MgO	42.68	41.22	43.40	0.15	41.16	42.81	42.49	0.13	41.04	44.78	38.20	0.11	0.13	17.44	17.23	27.84	0.17	0.11	26.30
CaO	0.17	0.19	0.18	10.25	0.18	0.18	0.21	9.67	0.18	0.06	0.21	10.27	10.55	14.24	16.38	1.77	11.50	9.96	2.06
Na2O	0.04	0.09	-	5.14	0.02	0.01	0.04	5.63	0.02	0.03	0.03	5.36	5.31	0.31	0.39	0.16	4.92	5.54	0.10
K_2O	0.02	0.01	-	0.53	0.03	-	0.05	0.59	0.01	0.02	0.01	0.38	0.35	0.03	0.02	0.08	0.31	0.40	0.01
NiO	0.29	0.22	0.23	0.04	0.25	0.22	0.25	-	0.27	0.35	0.29	0.03	0.04	0.06	0.00	0.14	0.01	0.03	0.01
P_2O_5	0.09	0.04	0.15	-	0.06	0.04	0.09	0.02	0.05	0.03	0.01	0.02	0.02	0.02	0.02	0.03	0.03	0.02	0.00
Total	101.07	101.32	99.92	99.54	100.88	100.08	100.85	99.62	100.69	100.43	100.93	99.73	99.64	99.60	99.79	100.16	99.86	99.73	99.59
Mg#	81.0	78.3	82.3	26.0	78.7	81.5	80.8	28.7	78.6	84.2	74.6	37.6	30.5	71.7	75.2	79.8	30.3	33.2	76.5
An	-	-	-	50.80	-	-	-	47.05	-	-	-	50.29	51.30	-	-	-	55.34	48.69	-
En	-	-	-	-	-	-	-	-	-	-	-	-	-	49.65	48.75	76.29	-	-	72.74
Fs	-	-	-	-	-	-	-	-	-	-	-	-	-	20.08	16.50	19.67	-	-	22.81
Wo	-	-	-	-	-	-	-	-	-	-	-	-	-	29.12	33.31	3.48	-	-	4.09
Fo	80.8	78.1	82.1	-	78.4	81.3	80.6	-	78.4	84.1	74.3	-	-	-	-	-	-	-	-

Note: Mg# =100*(MgO/40.31)/(MgO/40.31+FeO^T/71.85). C-core; r-rim.

Table DR2 Major (wt%) and trace elements (ppm) data for the Cenozoic high-Mg andesites in Russian Far East

Sample	17R19-1	17R19-2	17R19-3	17R19-4	17R19-5	17R19-6	17R19-7	17R19-8	17R20-1	17R20-2	17R20-3	17R20-4
SiO_2	55.76	55.99	55.42	55.48	55.57	55.84	55.66	55.71	55.47	55.61	56.79	57.34
TiO_2	1.69	1.69	1.64	1.65	1.66	1.68	1.67	1.67	1.48	1.50	1.55	1.57
Al_2O_3	14.97	15.01	14.86	14.90	14.87	14.98	15.01	14.93	14.64	14.61	14.93	15.03
Fe_2O_3	8.73	8.63	8.66	8.75	8.89	8.61	8.60	8.85	8.88	8.88	8.67	8.58
MnO	0.11	0.10	0.09	0.09	0.11	0.11	0.11	0.11	0.11	0.11	0.11	0.11
MgO	5.15	4.92	4.97	5.06	5.24	5.12	5.13	5.29	5.78	5.60	5.27	5.17
CaO	6.03	6.06	5.82	5.83	6.00	5.99	6.02	6.01	6.60	6.62	6.51	6.56
Na_2O	3.59	3.70	3.86	3.87	3.60	3.54	3.50	3.61	3.59	3.55	3.50	3.59
K_2O	2.73	2.61	2.38	2.39	2.66	2.91	2.90	2.75	1.57	1.63	1.94	1.93
P_2O_5	0.44	0.44	0.42	0.42	0.43	0.43	0.43	0.43	0.28	0.29	0.29	0.29
LOI	0.33	0.57	0.90	0.77	0.43	0.25	0.36	0.26	0.93	0.82	0.03	0.01
Total	99.51	99.73	99.01	99.20	99.46	99.46	99.39	99.63	99.32	99.23	99.59	100.18
Mg#	53.9	53.1	53.2	53.4	53.9	54.1	54.2	54.2	56.3	55.5	54.6	54.4
Na_2O+K_2O	6.32	6.31	6.24	6.27	6.26	6.45	6.41	6.36	5.15	5.18	5.44	5.52
Li	8.06	8.38	8.18	8.59	8.26	7.83	7.99	8.54	7.04	6.97	7.18	6.96
Be	1.39	1.38	1.38	1.46	1.48	1.47	1.52	1.44	1.30	1.32	1.33	1.43
Sc	11.1	11.0	10.9	11.0	10.9	10.9	11.3	11.3	12.1	12.2	12.6	12.6
V	125	126	124	127	125	125	127	127	136	138	139	141
Cr	160	160	154	159	162	164	164	167	212	197	199	201
Co	31.0	29.2	28.8	30.7	30.9	31.4	31.0	31.3	32.8	31.9	32.2	32.0
Ni	96.1	92.0	89.0	95.5	95.1	98.1	97.2	97.4	161	153	146	143
Cu	26.5	26.3	25.8	27.5	26.9	26.9	27.2	27.1	62.2	62.6	59.3	65.8
Zn	102	105	103	103	107	108	108	107	105	105	110	112
Ga	21.9	22.3	22.1	22.2	22.0	22.6	22.8	22.8	21.8	21.4	22.3	22.6
Rb	57.4	57.3	55.5	55.7	55.6	60.4	60.5	58.4	31.8	34.9	38.3	39.3
Sr	733	744	695	711	735	729	748	750	498	496	485	488
Y	17.9	18.3	17.6	17.8	18.1	18.2	18.3	18.3	15.9	16.1	17.1	17.3
Zr	158	160	152	157	158	158	161	160	138	141	154	158
Nb	25.4	25.8	24.8	25.6	25.9	25.4	25.8	25.9	14.4	14.9	14.9	15.0
Mo	1.02	1.04	0.83	0.89	1.00	1.10	1.10	1.27	0.78	0.83	0.92	0.88
Sn	2.08	2.13	2.20	2.19	2.07	2.08	2.05	2.17	1.77	1.86	2.00	2.07
Cs	0.73	0.75	0.58	0.57	0.74	0.84	0.83	0.78	0.23	0.26	0.42	0.44
Ba	759	772	745	767	771	779	790	778	472	486	468	485
La	27.2	27.7	26.3	27.2	27.1	27.2	27.8	28.0	21.3	21.7	22.3	22.8
Ce	56.1	57.6	54.5	56.3	56.8	56.8	58.1	57.8	42.6	43.3	44.9	45.9
Pr	6.91	7.07	6.57	6.83	6.88	6.90	6.88	6.86	5.03	5.16	5.42	5.53
Nd	29.6	29.8	28.4	29.2	29.7	29.4	30.1	30.3	21.7	22.0	23.3	23.5
Sm	6.44	6.49	6.38	6.68	6.43	6.57	6.67	6.49	4.83	4.97	5.39	5.43
Eu	1.87	1.86	1.85	1.95	1.88	1.93	1.98	1.90	1.54	1.56	1.58	1.65
Gd	5.39	5.42	5.31	5.36	5.40	5.59	5.54	5.46	4.26	4.36	4.70	4.81
Tb	0.75	0.76	0.73	0.77	0.75	0.74	0.73	0.77	0.62	0.64	0.66	0.70
Dy	3.89	3.87	3.87	3.99	3.94	4.17	4.03	4.03	3.27	3.49	3.67	3.58
Ho	0.66	0.67	0.63	0.66	0.66	0.64	0.67	0.67	0.56	0.57	0.63	0.65
Er	1.55	1.60	1.61	1.59	1.68	1.66	1.74	1.64	1.44	1.42	1.62	1.60
Tm	0.22	0.23	0.20	0.23	0.23	0.22	0.23	0.24	0.22	0.21	0.23	0.23
Yb	1.18	1.21	1.09	1.21	1.16	1.15	1.23	1.19	1.06	1.05	1.22	1.27
Lu	0.17	0.18	0.18	0.19	0.19	0.19	0.20	0.19	0.18	0.18	0.20	0.20
Hf	3.82	3.83	3.76	3.92	3.94	3.95	3.92	3.99	3.48	3.54	3.84	4.04
Ta	1.29	1.30	1.28	1.33	1.39	1.38	1.38	1.39	0.77	0.77	0.79	0.78
W	0.61	0.68	0.60	0.65	0.66	0.65	0.64	0.65	0.54	0.39	0.43	0.48
Tl	0.18	0.16	0.16	0.16	0.17	0.18	0.16	0.19	0.095	0.10	0.14	0.13
Pb	5.49	5.51	5.34	5.52	5.54	5.62	5.63	5.79	3.93	3.73	4.25	4.50
Th	3.16	3.24	3.02	3.09	3.24	3.16	3.20	3.26	1.73	1.83	1.83	1.93
U	0.78	0.78	0.73	0.72	0.79	0.77	0.79	0.79	0.36	0.38	0.36	0.37
Nb/U	32.45	32.96	33.98	35.51	32.70	32.81	32.65	32.73	39.60	39.47	40.85	40.55
Ce/Pb	10.22	10.44	10.19	10.19	10.25	10.11	10.33	9.99	10.84	11.62	10.56	10.21
$(La/Yb)_N$	15.60	15.38	16.31	15.22	15.67	15.88	15.22	15.82	13.59	13.87	12.29	12.13
$(La/Sm)_N$	2.66	2.68	2.60	2.56	2.65	2.60	2.62	2.71	2.77	2.74	2.60	2.64
ΣREE	141.96	144.44	137.61	142.19	142.78	143.15	145.92	145.57	108.65	110.58	115.71	117.80

Note: LOI: Loss on ignition; ΣREE=La+Ce+Pr+Nd+Sm+Eu+Gd+Tb+Dy+Ho+Er+Tm+Yb+Lu; $(La/Sm)_N$=(La/0.310)/(Sm/0.195); $(La/Yb)_N$=(La/0.310)/(Yb/0.209); Mg# =100*(MgO/40.31)/(MgO/40.31+FeOT/71.85).

Table DR3 Sr-Nd-Hf-Pb isotopes data of high-Mg andesites from Russian Far East.

Sample	17R19-1	17R19-2	17R19-3	17R19-4	17R19-5	17R19-6	17R19-7	17R19-8	17R20-1	17R20-2	17R20-3	17R20-4
$^{87}Sr/^{86}Sr$	0.705620	0.705629	0.705670	0.705690	0.705636	0.705632	0.705642	0.705701	0.705862	0.705834	0.705893	0.705890
1SE	0.000008	0.000007	0.000006	0.000009	0.000008	0.000007	0.000007	0.000010	0.000006	0.000009	0.000009	0.000006
$^{143}Nd/^{144}Nd$	0.512432	0.512428	0.512386	0.512411	0.512429	0.512416	0.512419	0.512417	0.512449	0.512463	0.512462	0.512447
1SE	0.000003	0.000003	0.000002	0.000003	0.000003	0.000003	0.000003	0.000003	0.000002	0.000002	0.000002	0.000003
ε_{Nd}	-4.0	-4.1	-4.9	-4.4	-4.1	-4.3	-4.3	-4.3	-3.7	-3.4	-3.4	-3.7
$^{176}Hf/^{177}Hf$	0.282640	0.282645	0.282654	0.282646	0.282656	0.282645	0.282652	0.282647	0.282698	0.282686	0.282683	0.282669
1SE	0.000002	0.000006	0.000002	0.000004	0.000003	0.000002	0.000003	0.000002	0.000003	0.000002	0.000002	0.000004
ε_{Hf}	-4.7	-4.5	-4.2	-4.5	-4.1	-4.5	-4.2	-4.4	-2.6	-3.1	-3.1	-3.7
$^{206}Pb/^{204}Pb$	17.1677	17.1846	17.1561	17.1530	17.1870	17.1637	17.1714	17.1866	16.8152	16.7572	16.7634	16.7692
1SE	0.0002	0.0001	0.0002	0.0001	0.0001	0.0002	0.0002	0.0001	0.0002	0.0002	0.0002	0.0001
$^{207}Pb/^{204}Pb$	15.4432	15.4463	15.4436	15.4443	15.4482	15.4462	15.4463	15.4484	15.4303	15.4256	15.4244	15.4257
1SE	0.0002	0.0002	0.0002	0.0001	0.0001	0.0002	0.0002	0.0001	0.0002	0.0002	0.0002	0.0002
$^{208}Pb/^{204}Pb$	37.0810	37.0997	37.0713	37.0718	37.1067	37.0846	37.0885	37.1063	36.7585	36.7132	36.7114	36.7181
1SE	0.0005	0.0004	0.0005	0.0003	0.0003	0.0004	0.0006	0.0003	0.0004	0.0004	0.0004	0.0004

Note: SE stands for standard error； $\varepsilon Nd=[(^{143}Nd/^{144}Nd)_{Sample}/(^{143}Nd/^{144}Nd)_{CHUR}-1]\times10^4$； $(^{143}Nd/^{144}Nd)_{CHUR} = 0.512638$；
$\varepsilon Hf=[(^{176}Hf/^{177}Hf)_{Sample}/(^{176}Hf/^{177}Hf)_{CHUR}-1]\times10^4$； $(^{176}Hf/^{177}Hf)_{CHUR} = 0.282772$.

Table DR4 Geochemical characteristics of some high-Mgandesites (wt.%) from subduction zone

Location	SiO_2	Al_2O_3	MgO	CaO	Na_2O+K_2O	Mg#	La/Yb
White Island,New Zealand	55.6	13.2	10.1	8.9	3.5	0.71	3.6
Amphlett Island,Papua New Guinea	54.3	14.8	8.7	7.6	5.2	0.67	–
Mount Shasta,Cascades	57.9	14.7	8.9	8.1	3.9	0.74	10.2
Setouchi Belt,Japan	58.5	13.3	9.5	6.1	3.9	0.73	9.1
Adak Island,central Aleutians	56.8	15.5	7.4	8.6	4.4	0.66	8.8
Piipvolcano,western Aleutians	57.0	16.0	6.6	7.7	4.8	0.72	4.6
Russian Far East	**55.4-57.3**	**14.6-15.0**	**4.9-5.8**	**5.8-6.6**	**5.2-6.4**	**0.53-0.56**	**18-23**

Data sources: Wood and Tuner (2009).

Table DR5 Compared Sr-Nd-Pb isotopic data from intraplate basalts in NE China and andesites in arc

Location	Lithology	Samp1e	$(^{87}Sr/^{86}Sr)i$	$(^{143}Nd/^{144}Nd)i/$ [δNd(t)]	$^{206}Pb/^{204}Pb$	$^{207}Pb/^{204}Pb$	$^{208}Pb/^{204}Pb$	Reference
Changbaishan	sodic basalts	HaKu-1a	0.705078	0.512537	17.379	15.538	37.743	Kuritani et al.,2009
		Haku-2	0.705181	0.512513	17.482	15.543	37.805	
		Haku-7	0.704956	0.512582	17.410	15.540	37.893	
		Haku-10	0.705008	0.512599	17.384	15.506	37.781	
		Haku-20	0.705319	0.512550	17.569	15.508	37.953	
		HaKu-25	0.704985	0.512555	17.390	15.535	37.627	
		Haku-26	0.705039	0.512555	17.378	15.538	37.625	
		Haku-27	0.704926	0.512642	17.824	15.537	38.244	
		Haku-30b	0.705018	0.512579	17.435	15.532	37.672	
		Haku-32b	0.705531	0.512554	17.614	15.541	38.087	
		Haku-34	0.705114	0.512583	17.657	15.543	38.008	
		Haku-35	0.704817	0.512586	17.373	15.526	37.564	
		Haku-36	0.704954	0.512619	17.604	15.545	37.845	
Longgang	sodic basalts	LG9940	0.704467	0.512665	17.9100	15.5700	38.3940	Kuritani et al.,2011
		LG99L11-1	0.704443	0.512674	17.9530	15.5560	38.4800	
		HJ97001A	0.704488	0.512663	17.9310	15.5460	38.4570	
		HAKU40	0.704418	0.512723	18.1417	15.5566	38.5694	
Shuangliao	sodic basalts	BBT-3	0.703298	0.512838 (5.2)	18.24	15.47	38.21	Xu et al., 2012
		BLS-5	0.70341	0.512892 (6.2)	18.13	15.50	38.18	
		DHLB-1	0.703526	0.512831 (5)	18.34	15.50	38.33	
		DHLB-8	0.703597	0.512854 (5.5)	18.28	15.50	38.34	
		DTJ-5	0.703609	0.512821 (4.6)	18.26	15.48	38.23	
		NBS-3	0.703043	0.512845 (5.3)				
		NBS-4	0.703254	0.512854 (5.4)	18.23	15.46	38.19	
		XHLB-1	0.703407	0.512811 (4.7)	18.39	15.56	38.58	
		XHLB-7	0.703353	0.51282 (4.8)	18.29	15.49	38.29	
		XTJ-1	0.703278	0.512798 (4.2)	18.21	15.48	38.21	
		XTJ-6	0.703311	0.512829 (4.8)	18.21	15.49	38.25	
Mt. Shasta, N California	andesites	85-48b	0.70275	7.4	18.798	15.589	38.407	Grove et al., 2002
		82-94a	0.70366	5.2	18.937	15.616	38.573	
		82-94d	0.70292	7.2	18.893	15.611	38.56	
		85-41b	0.70299	6.6	18.851	15.567	38.405	
		82-85	0.70375	4.5	18.96	15.595	38.579	
		85-59	0.70378	5.1	18.991	15.634	38.707	
Western Aleutian	andesites	Apr-16	0.7028	10.29	17.987	15.412	37.448	Yogodzinski et al.,1994
		V35/G5B	0.70264	10.19	18.089	15.431	37.535	
		V35/G5A	0.70265	10.64	18.081	15.43	37.539	
		V35/G4X1	0.70269	10.64	18.063	15.422	37.487	
		V35/G9D	0.70257	10.48	18.165	15.422	37.56	
		V35/G7C	0.70269	10.44	18.161	15.438	37.594	
		V35/G7A	0.70276	11.15	18.015	15.42	37.449	

Table DR6 Present-day compositions of the end-member components

Component	1.5 Ga pelagic sediments	Recent Pacific sediments	Depleted mantle
Sr, ppm	189	189	7.66
Nd, ppm	46	46	0.58
Pb, ppm	18	18	0.02
$^{87}Sr/^{86}Sr$	0.72030	0.70954	0.70369
$^{143}Nd/^{144}Nd$	0.51170	0.51234	0.51285
$^{206}Pb/^{204}Pb$	16.757	18.827	17.645
$^{207}Pb/^{204}Pb$	15.478	15.672	15.398
$^{208}Pb/^{204}Pb$	37.239	39.395	37.360

Data from Kuritani et al. (2011).